A Switched-mode Self-sensing Solution for Piezoelectric Synchronous Electric Charge Extraction (SECE)

Linglong Gao, *Graduate Student Member, IEEE*, Li Teng, *Graduate Student Member, IEEE*, Minfan Fu, *Senior Member, IEEE*, Haoyu Wang, *Senior Member, IEEE*, and Junrui Liang, *Senior Member, IEEE*

***Abstract*—In piezoelectric energy harvesting (PEH), utilizing the synchronized switch interface circuit can significantly enhance the energy harvesting capability. Vibration sensing is necessary for carrying out the synchronized switch actions. The peak detection was usually implemented with an external displacement sensor in the early designs, which was not compatible with self-contained and integrated applications. This paper proposes a compact self-sensing synchronized switch interface for PEH by using a modified buck-boost topology and implementing a time-sharing control on it. The interface circuit works in strong discontinuous conduction mode (DCM). The sensing function is realized by extracting a tiny amount of charge from the piezoelectric transducer, which introduces little influence to the piezoelectric source. While the energy harvesting function is realized by extracting charge at a higher intensity. The two functions cooperate in a time-sharing way. The sensed full-cycle information is used to identify the voltage peaks, at which the switch actions are synchronously carried out. The self-sensing mechanism is studied theoretically and experimentally. In the experiments, the self-sensed information of the piezoelectric voltage matches the measured result. The peak detection is well performed. The newly proposed self-sensing mechanism offers a more informative and flexible solution for the designs of synchronized switch interface circuits.**

***Index Terms*—Self-sensing, time-sharing control, energy harvesting, piezoelectric materials, vibration.**

I. Introduction

The piezoelectric materials are widely applied in industrial applications to fabricate electromechanical transducers. Through piezoelectric transducers, the electrical signal can be converted into vibration or sound, and vice versa. As a result, the dynamic information of a piezoelectric structure can be sensed in the form of an electrical signal. The electrical signal can be further digitized and processed. Based on this principle, motion sensors such as accelerometers are fabricated. Accelerometers can be applied in motion sensing and smart wearable devices. Besides, the energy associated with the mechanical vibration can also be transformed into electrical energy via the piezoelectric elements. Piezoelectric energy harvesting (PEH) technology is developed based on this principle. The harvested energy can be used to energize the low-power electronics toward more battery-free internet of things (IoT) devices [2]–[5]. It can reduce the maintenance cost, especially when those devices are massively distributed in some wide-range and/or long-lasting applications, such as bridges, railways, and power grids [4], [6].

In addition to supplying energy, in some designs, the piezoelectric transducer also works as a motion sensor. With the help of the direct piezoelectric effect, in their design, Chew et al. used a single piezoelectric transducer as the strain sensor and energy harvester [7]. These two functions are realized by using two independent circuit modules. When enough energy is harvested and stored, the voltage of the transducer is sensed by an analog-to-digital converter (ADC) in the wireless sensing embedded system. The sensed result is further processed to reflect the dynamic strain information.

The full-wave and half-wave bridge rectifiers are the most extensively used piezoelectric interface circuits. It rectifies the ac voltage into the dc form [8], [9]. The interface circuit utilizing a full-wave diode bridge is called the standard energy harvesting (SEH) circuit. The maximum power of SEH is limited because of the negative power in a vibration cycle. The synchronized switch technology is proposed as a special power factor correction (PFC) technology for piezoelectric energy harvesting (PEH) enhancement [10]. The most representative topologies include synchronized switch harvesting on inductor (SSHI) [11], [12] and synchronous electric charge extraction (SECE) [13].

To further enhance the PEH capability, the multi-step bias-flip and charge extraction schemes have been proposed [14], [15]. These methods can reduce the inductor current peak, such that to reduce the power dissipation in the equivalent series resistance (ESR). Although the maximum harvested power of SSHI is higher than that of SECE [16], [17], SECE has an advantage of load independence [18]. Some up-to-date designs were developed based on the principle of synchronized charge extraction. For example, synchronous inversion and charge extraction (SICE) outperforms the previous designs by alternately combining one charge extraction with several

This work was supported in part by the Natural Science Foundation of Shanghai under Grant 21ZR1442300; in part by National Natural Science Foundation of China under Grant U21B2002. This article is an extended version of the paper presented in part at the 2021 IEEE Applied Power Electronics Conference and Exposition (APEC) [1]. (*Corresponding authors: Junrui Liang*).

Linlong Gao is with the School of Information Science and Technology, ShanghaiTech University, Shanghai 201210, China, also with the Shanghai Advanced Research Institute, Chinese Academy of Sciences, Shanghai 201210, China, and also with the University of Chinese Academy of Sciences, Beijing 100049, China. (e-mail: gaoll1@shanghaitech.edu.cn).

Li Teng, Minfan Fu, Haoyu Wang, and Junrui Liang are with the School of Information Science and Technology, ShanghaiTech University, and Shanghai Engineering Research Center of Energy Efficient and Custom AI IC, Shanghai 201210, China. (e-mail: fumf@shanghaitech.edu.cn, wanghy@shanghaitech.edu.cn, tengli@shanghaitech.edu.cn, liangjr@shanghaitech.edu.cn).

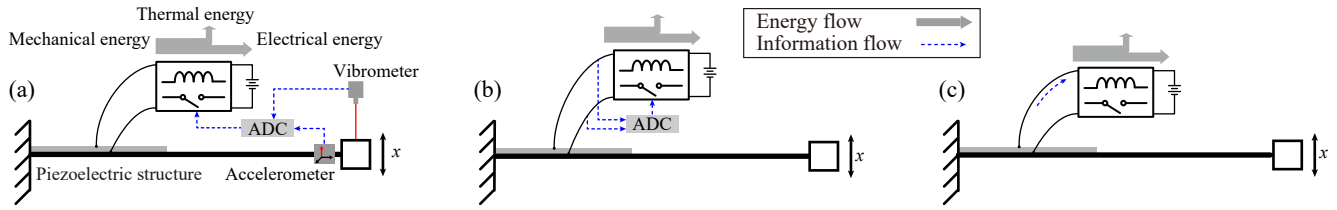

Fig. 1. Different sensing solutions in synchronized switch PEH. (a) Using additional motion sensors; (b) Using piezoelectric element as a sensor and an ADC module for digitization; (c) The proposed design, using piezoelectric element as a sensor and switched-mode circuit for quanitification.

bias-flip actions in some sequent synchronized instants [16]. Multiple charge extractions with bias- flip (MCEBF) provides another improvement by extracting a part of the charge and flipping the remaining charge at each synchronized instant [19]. Some synchronized switch solutions were implemented on integrated circuit (IC) chips [15], [20]–[23] to reduce the circuit size. As the volume of the inductor is much larger than other electronic devices in the synchronized switch solutions, some inductor-less IC solutions were proposed to reduce the inductor by using switched-capacitor technology [24]–[26].

The sensor is not only an important part of the IoT devices but also indispensable in the synchronized switch PEH technology for carrying out proper switching actions toward higher harvesting capability. The most straightforward solution for synchronization is to refer to the signal from an external motion sensor [27]. In the previous studies, the utilized motion sensors include laser vibrometer, approximation sensor, accelerometers, etc., as illustrated in Fig. 1(a). On the other hand, it was known that a piezoelectric transducer itself can also serves as a sensor. The open-circuit voltage is propotional to the deformation of the piezoelectric element. In some designs, the pieoelectric element is used as a sensor in some vibration cycles and as an energy harvester in the other cycles by toggling two independent circuit modules. In these designs, a commercial ADC is used to digitize the piezoelectric voltage in the sensing mode [28], [29]. The system diagram of these solutions is illustrated in Fig. 1(b).

In this paper, we propose a new self-sensing solution based on volt-second balance, an inherent characteristic of switched-inductor power electronics. The voltage quantification and switch control can be implemented using a low-cost microcontroller, which has a fundamental timer module. The system diagram of the proposed design is illustrated in Fig. 1(c). The sensing and energy harvesting functions are carried out by using the same interface circuit, but different control strategies.

II. Switched-mode Self-sensing Principle

SECE is one of the most extensively investigated interface circuits for PEH enhancement. Its circuit topology is illustrated in Fig. 2(a). SECE consists of two parts: a full-wave bridge rectifier and a charge extraction circuit. The full-wave diode bridge rectifies the input current following into the charge extraction stage to the same direction. The charge extraction circuit transfers all the charge in the piezoelectric capacitor C_p to the load side through an inductor L_i at each synchronized instant, where a voltage extreme (peak or valley) is attained. Without charge extraction, the remaining charge in C_p will be

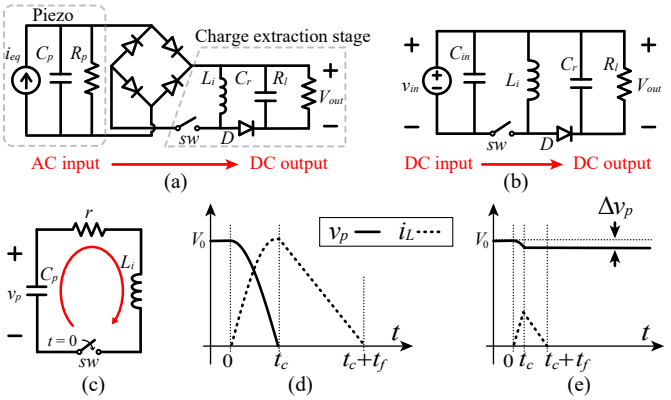

Fig. 2. SECE circuit and transient waveform. (a) SECE circuit. (b) Conventional buck-boost dc-dc converter for comparison. (c) Transient r-L_i-C_p circuit. (d) Waveform in full charge extraction (conventional SECE process). (e) Waveform in tiny charge extraction.

neutralized in the following half vibration cycle. The charge extraction circuit in SECE is similar to the dc-dc buck-boost converter, whose topology is illustrated in Fig. 2(b). The inductor L_i in SECE plays the same role as that in buck-boost converter. It conveys energy from the input source to the load in an isolating way. Since the charge extraction is carried out almost instantaneously, it works in a strong discontinuous conduction mode (DCM). The difference is that, in SECE, the piezoelectric capacitance C_p is small; therefore, the voltage encounters a rapid transient drop to zero. While in the conventional buck-boost dc-dc converter, the input capacitance is relatively large. Therefore, the voltage changes very little after the charge extraction. No matter for the SECE or buck-boost converter, during the sw turn-on interval, the equivalent circuit is a transient underdamped RLC circuit, which is formed by the piezoelectric capacitance C_p, inductance L_i and equivalent series resistance (ESR) r, as shown in Fig. 2(c).

Fig. 2(d) shows the waveform in a normal SECE process. Given the piezoelectric voltage starts from $v_p(0) = V_0$. The transient voltage $v_p(t)$ and inductor current $i_L(t)$ are expressed as follows

$$v_p(t) = V_0 e^{-\zeta\omega_n t}\cos(\omega_d t - \varphi),\ 0 \le t < T_{\mathrm{RLC}}/4; \quad (1)$$

$$i_L(t) = -V_0 C_p \omega_n e^{-\zeta\omega_n t}\cos(\omega_d t - \varphi - \theta),\ 0 \le t < T_{\mathrm{RLC}}/4, \quad (2)$$

where

$$\omega_n = \frac{1}{\sqrt{L_i C_p}}, \quad \omega_d = \omega_n\sqrt{1-\zeta^2} \quad (3)$$

are the natural frequency and resonant frequency of the

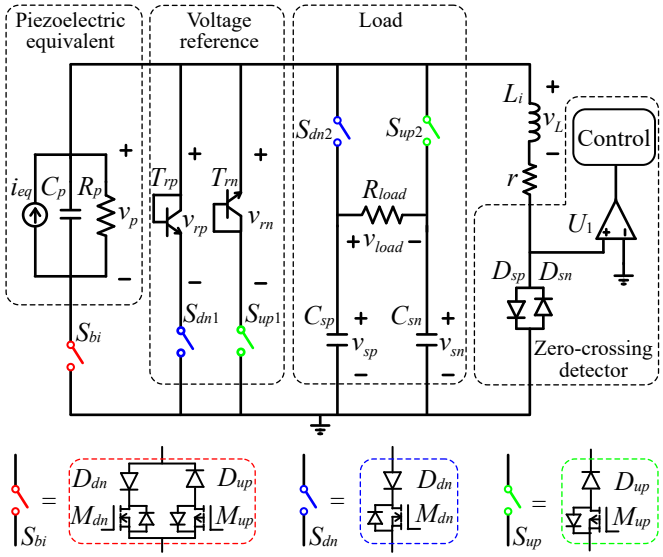

Fig. 3. Switched-mode self-sensing SECE circuit.

circuits, respectively;

$$T_{\text{RLC}} = \frac{2\pi}{\omega_d}, \tag{4}$$

is the RLC cycle of the r-L_i-C_p transient circuit;

$$\varphi = \tan^{-1}\frac{\zeta}{1-\zeta^2}, \quad \theta = \cos^{-1}\zeta. \tag{5}$$

are two phase differences. The damping factor ζ is inversely proportional to the quality factor Q with the following relation

$$\zeta = \frac{1}{2Q} = \frac{r}{2}\sqrt{\frac{C_p}{L_i}}. \tag{6}$$

In a normal SECE action, the transient switch sw conducts for an interval of $T_{\text{RLC}}/4$.[1] At the end of this switch-on interval, the piezoelectric voltage v_p approximately arrives at zero, as illustrated at t_c instant in Fig. 2(d). All charge in C_p is extracted and transferred to the capacitor C_r through the inductor L_i.

On the other hand, when the sw conduction interval is much smaller than $T_{\text{RLC}}/4$, as illustrated in Fig 2(e), a small amount of electric charge in the piezoelectric capacitor C_p is transferred to the inductor L_i. The voltage across the piezoelectric capacitor v_p only changes a little bit, i.e., Δv_p. In addition, the derivative of the inductor current at the switch-on instant can be formulated from (2) as follows

$$\left.\frac{\mathrm{d}i_L}{\mathrm{d}t}\right|_{t=0} = \frac{V_0}{L_i}. \tag{7}$$

The current waveform in tiny charge extraction is almost the same as that in the buck-boost converter, i.e., magnitizing the switched inductor with a constant voltage, under strong DCM operation. Given a sufficiently small switch-on interval, the volt-second balance principle approximately holds for a piezoelectric source. Therefore, the product of piezoelectric voltage v_p and the tiny piezoelectric charge extraction interval t_c (also the magnitizing interval of L_i) equals to that of reference constant voltage V_r and the freewheeling interval t_f, i.e.,

$$\lim_{t_c\to 0} v_p(0)t_c = V_r t_f. \tag{8}$$

Providing a constant V_r, the measurement value of piezoelectric voltage $\hat{v}_p$ can be calculated by learning from the proportional relation between the tiny charge extraction and freewheeling times, i.e.,

$$\hat{v}_p = \frac{V_r t_f}{t_c}. \tag{9}$$

Compared with the direct voltage quantification using ADC module, the proposed self-sensing solution has two benefits:

- It reuses the same charge extraction module to realize the sensing function; therefore, it is more compact. No additional module and auxiliary circuit is needed.
- It is not necessary to consider the voltage limit or the polarity issue as most ADC solution does.

This switched-mode self-sensing solution well fits the piezoelectric sources, which are featured as high-voltage, bipolar ac, and capacitive output.

III. Circuit Implementation

A. Topology

Based on the self-sensing principle mentioned in Section II and considering the polarity and control issues, the circuit topology of proposed switched-mode self-sensing SECE circuit is illustrated in Fig. 3. This design includes four sorts of branches: piezoelectric ac source, positive/negative voltage references, positive/negative rails (storage capacitors), and inductor branch for energy delivery. All energy flows go through the inductor branch from the source to the storages. All voltage information is generated in the inductor branch by comparing the piezoelectric voltage with the absolute reference voltages. The ac source branch is connected to the inductor branch by a bidirectional switch S_{bi} (in red), as shown in Fig. 3). Either of the reference voltage branches or energy storage branches is connected by a unidirectional switch. Switches S_{dn} in blue only allow downward current, while those S_{up} in green only allow upward current.

The principle of voltage quantification is based on the relationship described in (9) . An absolute and constant voltage source is necessary for providing a reliable voltage reference. The voltage across the load is not a good choice because of its fluctuation. In this design, we utilize the forward-bias voltage of a diode-connected transistor for providing an absolute voltage reference. Given the diode equation as follows

$$i_d = I_s\left[e^{v_d/(nV_T)} - 1\right], \tag{10}$$

the dynamic resistance of a normal diode, which is also known as the changing rate of v_d under different i_d, is expressed as follows

$$R_d(v_d) = \frac{\mathrm{d}v_d}{\mathrm{d}i_d} = \frac{nV_T}{I_s}e^{-v_d/(nV_T)}. \tag{11}$$

[1]The underdamped RLC branch usually has a high Q or equivalently low damping ratio; therefore, $\omega_d \approx \omega_n$. In practice, The $T_{\text{RLC}}/4$ interval can be more properly obtained through measurement.

It approaches zero rapidly under a large v_d. Therefore, the simplest model of a diode usually only considers a constant forward voltage drop. On the other hand, for a diode-connected transistor, given a gain β between the collector and base currents, the dynamic resistance can be expressed as follows

$$R_d(v_d) = \frac{\mathrm{d}v_d}{\mathrm{d}i_d} = \frac{nV_T}{(1+\beta)I_s} e^{-v_d/(nV_T)}. \tag{12}$$

Comparing (11) and (12), the equivalent resistance of the diode-connected transistor is even smaller, under a high current gain β. It further approaches the feature of an ideal constant voltage source. Therefore, in this study, we use two diode-connected transistors to provide positive and negative absolute voltage references for sensing implementation.

As shown in (9), the voltage estimation relies on an absolute reference voltage V_r and accurate time counts on the tiny charge extraction interval t_c and freewheeling interval t_f. t_c is actively controlled by a microcontroller. While t_f is an essential parameter to be sensed. It is obtained by detecting the zero-crossing instant of the inductor current. The zero-crossing comparator requires a high current-to-voltage gain, when the current is very close to zero. In a general current testing design, a small sampling resistor is connected in series to sample the current value. However, if we increase the resistance in order to enlarge the current-to-voltage gain (resistance) under the small current condition, the Joule dissipation under relative large current condition during the full charge extraction also increases. In this design, we use the nonlinear sampling diodes D_{sp} and D_{sn} for realizing large resistance under small current condition and small resistance under large current condition. The configuration for current sampling and zero-crossing detection is shown in the inductor branch of Fig. 3.

B. Time-sharing Control and Peak Detection

Based on the circuit topology shown in Fig. 3, the piezoelectric voltage can be sensed in any instant throughout a vibration cycle. On the other hand, voltage peak detection is realized by analyzing the sensed data, such that charge extraction actions can be carried out at the voltage peak instants. Fig. 4 shows the waveform and control flow chart of the proposed switched-mode self-sensing SECE.

The sensing actions are carried out with a constant sampling interval t_s, which is illustrated by the red pulses in the inductor current i_L waveform, as shown in Fig. 4(a). t_s is usually selected much smaller than a vibration cycle, such that more details of the piezoelectric voltage v_p can be measured. The sensed results are stored in the microcontroller for vibration analysis, in particular, identifying the voltage peaks for synchronous charge extraction. Three sequential sensing results can be used to determine whether v_p arrives at a peak position. A voltage peak is attained when the following criteria is satisfied

$$\text{sign}\left[\hat{v}_{p,(n-1)} - \hat{v}_{p,(n-2)}\right] = -\text{sign}\left[\hat{v}_{p,(n)} - \hat{v}_{p,(n-1)}\right], \tag{13}$$

where $\hat{v}_{p,(n)}$ is the measurement result of the n^{th} sample. There is a small delay between the actual peak and detected peak.

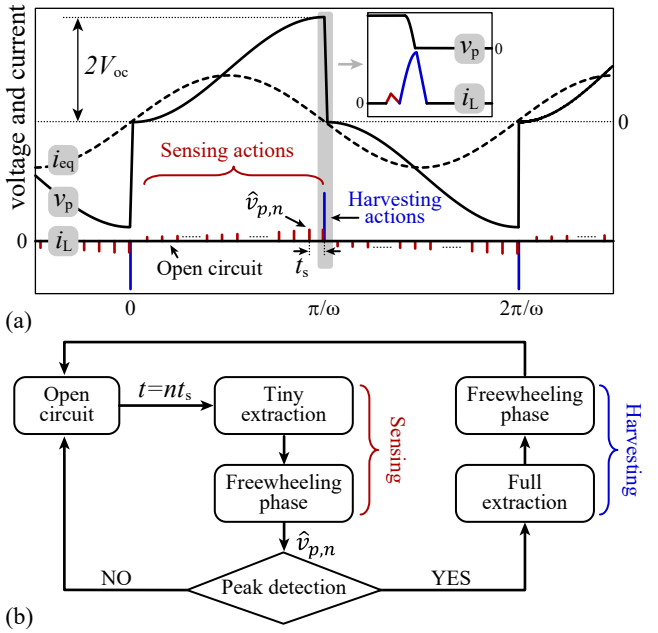

Fig. 4. Waveform overview and control of the proposed self-sensing SECE. (a) Waveform under time-sharing control. (b) Control flow chart.

Such a delay is a commonly seen in other peak detection designs [30].

Once a voltage peak position is detected, the charge extraction action is carried out immediately for energy harvesting purpose. The extracted charge also go through the inductor L_i to the storage. But different from the tiny charge extraction in sensing, it is a full charge extraction for energy harvesting. The high i_L pulses in blue illustrate the inductor current during charge extraction actions in Fig. 4(a). Because of the full charge extraction, the piezoelectric voltage v_p drops to zero. The extracted charge freewheels to the positive or negative rail (storage) eventually.

As we can see from the waveform and control scheme of this proposed switched-mode sensing method shown in Fig. 4, the sensing and harvesting actions are carried out independently. Both information acquisition and energy delivery functions can be realized simultaneously in a time-sharing way by using the same set of switched circuit branches.

C. Detailed Working Phases

To better illustrate the operation details of the proposed design, Fig. 5 shows five of the key working phases in a half positive v_p vibration cycle. The five representative phases include: open-circuit (Fig. 5(a) and (b)), tiny charge extraction (Fig. 5(c) and (d)), freewheeling in sensing (Fig. 5(e) and (f)), full extraction (Fig. 5(g) and (h)), and freewheeling in energy harvesting (Fig. 5(i) and (j)).

1) Open-circuit: During the positive v_p half cycle, in most of the time, the circuit works in these open-circuit phases. The conducting branches of this phase are shown in red in Fig. 5(b). Two open-circuit phases are separated by two sequential tiny charge extraction and freewheeling in sensing phases. All electronic switches turn off during the open-circuit phases. Only the equivalent ac source i_{eq} charges the piezoelectric

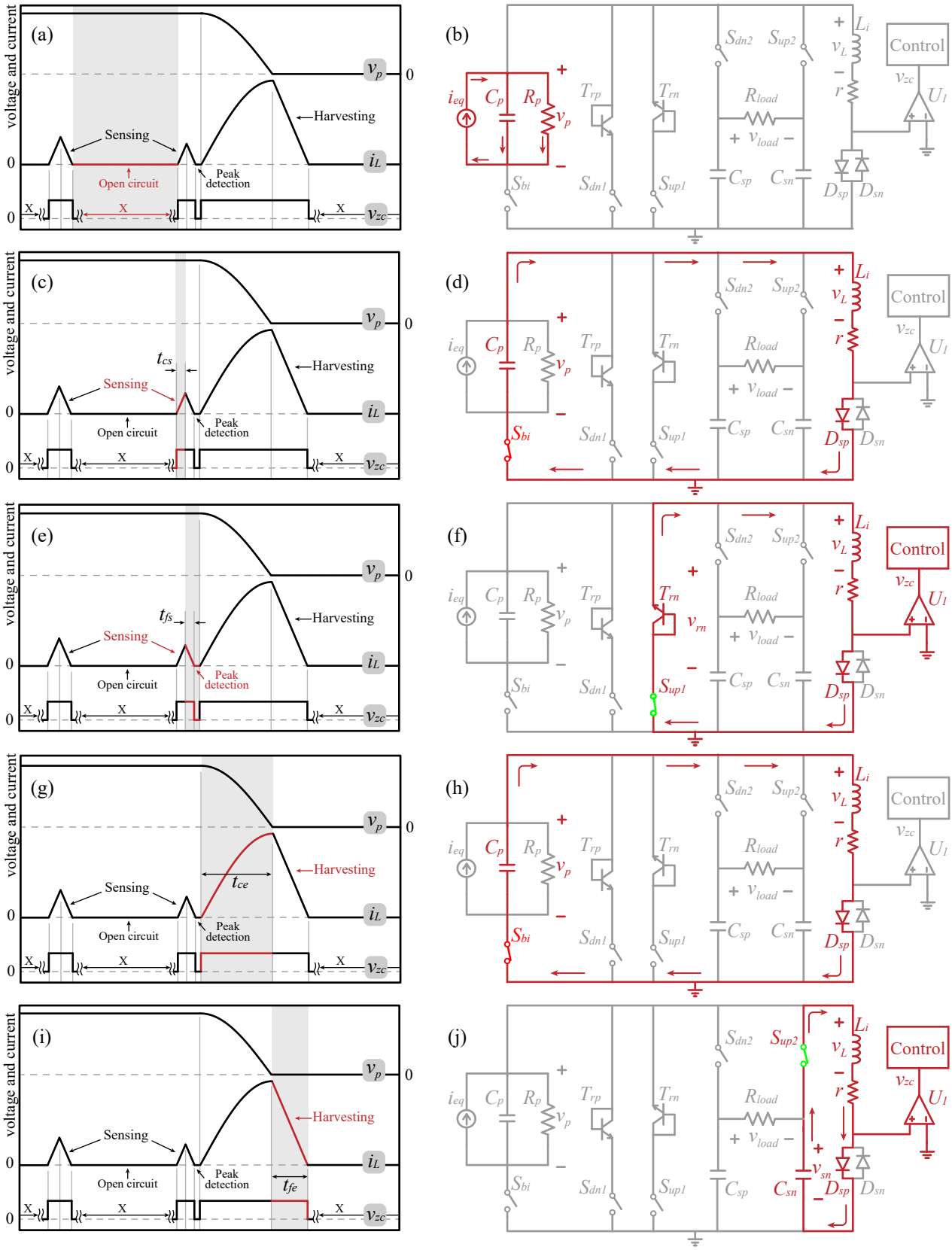

Fig. 5. Five of the key working phases in half of a vibration cycle. (a), (c), (e), (g), and (i) Waveform. (b), (d), (f), (h), and (j) Activated circuit branches. (a) and (b) Open-circuit. (c) and (d) Tiny charge extraction for sensing. (e) and (f) Freewheeling in sensing. (g) and (h) Full charge extraction for energy harvesting. (i) and (j) Freewheeling in energy harvesting.

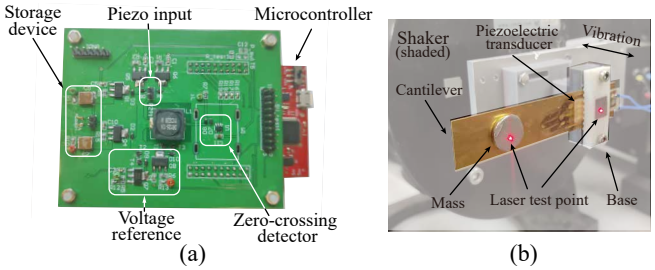

Fig. 6. Experimental setup. (a) PCB prototype; (b) Piezoelectric structure.

capacitor C_p. Since there is no current flowing through the inductor branch, v_{zc} the output voltage of the zero-crossing detector remains in an unknown state, which is marked "x" in the waveform shown in Fig. 5(a). Since v_{zc} is not used by the embedded program during these phases, the unknown state does not matter.

2) Tiny Charge Extraction: When the timer records a multiple of the sampling period t_s, the circuit carries out a sensing action by starting a tiny charge extraction phase. From the conducting branches shown in Fig. 5(d), the bidirectional electronic switch S_{bi} turns on for a very short interval t_{cs}. Only a tiny percentage of charge stored in C_p is extracted by the inductive branch. The piezoelectric voltage v_p is hardly affected. During this phase, the inductor current rises approximately with a constant time rate $(v_p - 2V_d)/L_i$, where V_d is the forward voltage drop of a diode. The diodes used in this design are all necessary for realizing either current sampling or current steering. As a small current flows through the inductor path, v_{zc} the output voltage of the zero-crossing detector reads high.

3) Freewheeling in Sensing: When a tiny charge extraction ends after a predefined interval, a freewheeling phase begins. In this phase, switch S_{up1} turns on until the inductor current, which freewheels through the diode-connected transistor T_{rn}, drains out. The waveform and conducting branches are shown in Fig. 5(e) and (f). As a small current flows through two diode and one diode-connected bipolar junction transistor (BJT), the inductor current drops with a constant time rate $-(V_r + 2V_d)/L_i$. V_r here is the forward voltage drop of the diode-connected transistor, which is taken as the voltage reference in sensing. When the inductor current crosses zero, the zero-crossing detector output reads a falling edge, which indicates the end of the freewheeling phase. At this moment, the duration of freewheeling interval t_{fs} is recorded by the microcontroller. The piezoelectric voltage v_p at this very moment, therefore, can be estimated according to (9) as follows

$$\hat{v}_p = \frac{t_{fs}}{t_{cs}}(V_r + 2V_d) + 2V_d. \tag{14}$$

In addition, the sensing results throughout a vibration cycle are recorded and processed by the microcontroller, in order to catch the voltage peak positions.

4) Full Charge Extraction: After every sensing action, the microcontroller inspects whether a voltage peak is attained according to (13). Once a peak is identified, a harvesting action is carried out right after this sensing action. The first phase in a harvesting action is full charge extraction. The waveform and conducting branches are illustrated in Fig. 5(g) and (h), respectively. The conducting branches are the same as those in the tiny charge extraction phase in Fig. 5(d). The switch-on interval is $T_{\text{RLC}}/4$, as the conventional SECE action, such that all charge stored in C_p is extracted. All energy is transferred to the inductor L_i. The piezoelectric voltage v_p drops to zero.

5) Freewheeling in Energy Harvesting: After all energy in C_p is transferred to L_i, S_{bi} opens and S_{up2} closes. The current in L_i freewheels through the negative-rail storage capacitor C_{sn}. When this freewheeling phase for charge extraction ends, the circuit enters a negative v_p half cycle. The operation and conducting branches in different phases of the negative v_p half cycle are symmetric to the aforementioned five phases in the positive v_p half cycle.

TABLE I
PARAMETERS OF THE EXPERIMENTAL SETUP.

Parameter	Value/Type	Parameter	Value/Type
Piezo patch (PZT)	$38 \times 12 \times 0.2$ mm^3	f_0 (Vibration)	35.1 Hz
Cantilever	$100 \times 20 \times 0.5$ mm^3	f_s (Sampling)	800 Hz
Displacement	2 mm (peak-to-peak)	C_p	50 nF
NMOS	ZVN4424GTA	NMOS $R_{ds(on)}$	4.3 Ω
PMOS	ZVP4424GTA	PMOS $R_{ds(on)}$	8.8 Ω
L_i (@2kHz)	100 mH	r (@2kHz)	160 Ω
BJTs	2SC4083T106N	C_{rp}, C_{rn}	10 μF
Diodes	NSR0240H	V_r (@1 mA)	0.72 V
Comparator (U_1)	TLV3201	V_d (@1 mA)	0.23 V
Microcontroller	TM4C123GXL	Probe resistance	20 Ω

IV. EXPERIMENTS

A. Setup

To validate the proposed design, an experimental setup is built. It is composed of a printed circuit board (PCB) and a piezoelectric structure, as illustrated in Fig. 6. The corresponding specifications are listed in Table I. A piezoelectric patch near the fixed end of the cantilever is connected to the switched-mode self-sensing SECE circuit. The base vibration is generated by a shaker, which is controlled and driven by a signal generator and a voltage amplifier. A differential laser vibrometer records the beam deflection information, providing a ground-truth reference for switched-mode sensing. A microcontroller is used to perform all the sensing, peak detection, and energy harvesting tasks. In this study, we emphasize the functional validation of the proposed switched-mode self-sensing design, the whole system has not realized self-powering capability yet. The control unit is powered by a USB cable, which is connected to a PC. The estimated information of v_p is processed by the microcontroller to identify the peak moments and sent to the PC through the same USB cable.

B. Functional Validation

The SECE function is implemented by the proposed switched-mode self-sensing solution. The sampling frequency in sensing is preset at $f_s = 800$ Hz with an internal timer of the

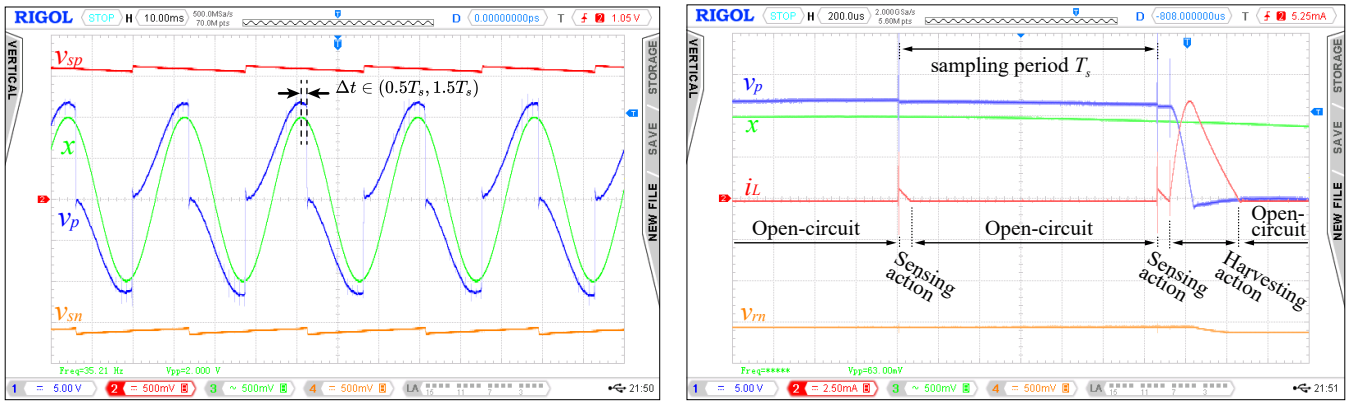

(a) (b)

Fig. 7. Experimental waveform. (a) Overview. (b) Enlarged view around a synchronized instant.

microcontroller. The global waveform of self-sensing SECE is illustrated in Fig. 7(a). As we can observe from the waveform, the synchronous instants for electric charge extraction are correct at the voltage (blue line) and displacement (green) peaks with a small phase lag. The small phase lag is due to the difference between a peak-extraction moment and the corresponding peak-recognition instant, which is approximately within $0.5T_s$ to $1.5T_s$ given a pure harmonic displacement ($T_s = 1/f_s$ is the sampling period). The voltage across positive (v_{sp} in red) or negative (v_{sn} in red) storage devices rises in immediate jumps at the electric charge extraction instants. During the open-circuit and sensing phases, the storage voltage gradually drops due to load consumption. The storage voltages arrive at a steady state when the energy gain equals to the consumption in a vibration cycle.

Fig. 7(b) shows the enlarged view around one of the synchronous full charge extraction instants. The smaller triangles in i_L waveform correspond to the sensing actions. It agrees with the theoretical design shown in Fig. 5(c)-(f). Given the tiny charge extraction in sensing, only a tiny drop is observed in the v_p curve (blue one Fig. 7(b)) during the sensing moment. When the peak voltage is detected, a harvesting action associated with a larger triangular i_L is carried out. v_p drops to zero under this full charge extraction. v_{sn} the negative-rail storage voltage rises during the current freewheeling.

C. Sensing Result

Full-cycle sensing capability is the unique feature of this proposed design, which was unprecedented in the previous studies. Fig. 8 shows the comparison of the sensed v_p with this switched-mode self-sensing method and the oscilloscope. As we can observe, when v_p is at a relatively high level above 3 V, the two sensing results match quite well. However, under 3 V, there are some mismatched points. The mismatch is caused by the non-ideal voltage references, which are realized with low-cost passive components. When the freewheeling current is small, the reference voltage can no longer be considered as approximately constant. Its value is smaller than that in the large current case. As the piezoelectric open-circuit voltage in most previous studies is much higher than 3 V, the sensing

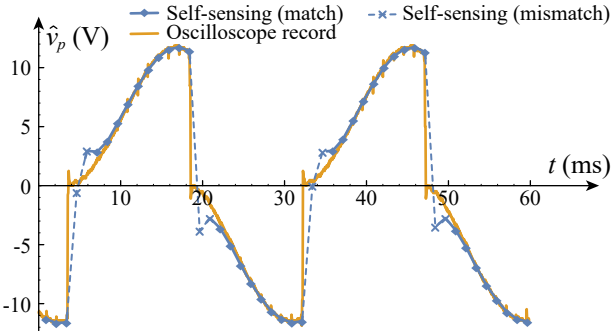

Fig. 8. Comparison of the sensing results.

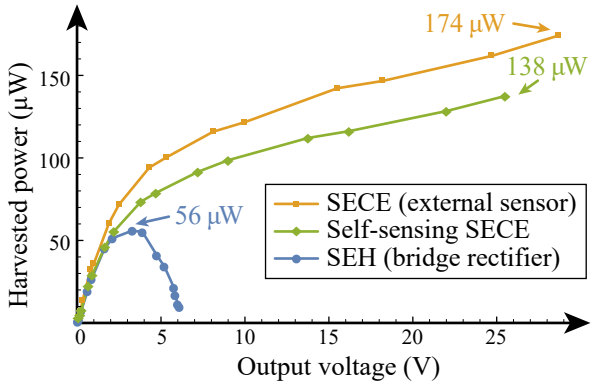

Fig. 9. Harvested power comparison.

mismatches under small v_p do not significantly affect the peak detection in most cases. But for a more universal self-sensing application, it is definitely an issue. A better solution will be considered in the future study.

D. Harvested Power

In the proposed solution, the switch control is not a self-powered version yet; the hardware and software of the embedded microcontroller were not strictly optimized according to the ultra-low-power criteria at this stage. On the other hand, we should not simply compare this self-sensing solution to the existing self-powered SECE, in terms of energy sustainability.

TABLE II
POWER LOSS BREAKDOWN.

Component		Power loss (μW)	Percentage
S_{bi}	$R_{ds(on)}$	1.18	1.92%
	Diodes	8.21	13.4%
Inductor path	ESR	34.9	56.9%
	Diodes	10.3	16.83%
	R_{probe}	4.37	7.12%
S_{up2}, S_{dn2}	$R_{ds(on)}$	0.24	0.39%
	Diode	2.11	3.43%
Total		61.3	100%

Because the functionality has been expanded to a new level in this study. It is the first design to realize full-cycle sensing, peak identification, and SECE harvesting function simultaneously. Functionality is emphasized in this initial proposal.

Putting the implementation effort of switch control aside, the harvested power is investigated to prove that the switched-mode full-cycle sensing does not sacrifice much of the harvesting performance. Fig. 9 compares the harvested power with different interface circuits including SEH, SECE using an external sensor, and the proposed self-sensing SECE, in this experiment, where the piezoelectric structure is weakly coupled. From the power comparison, the SECE using an external sensor or self-sensing solution significantly outperforms the SEH interface circuit. Ideally, given a weakly coupled system, the improvement of SECE is up to 300% compared with SEH, in terms of maximum harvested power. In this experiment, the improvements by using externally-sensing SECE and self-sensing SECE are 211% and 146%, respectively. It makes sense that the self-sensing solution pays a price for this convenient, self-contained, and more informative implementation. The energy harvesting enhancement of this solution is still significant, compared to the benchmarked SEH circuit.

Table II shows more details about the power losses in the circuit. The power consumptions of different components are estimated according to the inductor current i_L extracted from a circuit simulation tool. A probe resistor R_{probe} is inserted to sample the inductor current. As the power breakdown shows, the most power loss is consumed in the inductor path. The power loss of the single-directional switch is a relatively tiny part because the freewheeling interval is much shorter than the charge extraction interval under high output voltage.

V. CONCLUSION

This paper proposed a novel switched-mode self-sensing solution for piezoelectric energy harvesting (PEH) using a synchronized electric charge extraction (SECE) interface circuit. The voltage-sensing function is realized with the same buck-boost charge extraction circuit, based on the volt-second balance principle. The hardware topology enabling this self-sensing SECE is composed of several circuit branches, including a piezoelectric source, two absolute voltage references, positive and negative rails/storages, and an inductive branch with zero-crossing detection capability for intermediate energy delivery. By implementing a time-sharing control in this circuit with a microcontroller, the proposed circuit can perform scheduled voltage sampling, voltage peak detection, and full charge extraction at voltage peaks. Experimental results validated the functionality of this proposed design. It can realize full-cycle sensing, which is unprecedented in the previous PEH designs. Although some detailed issues, such as the sensing mismatch under low piezoelectric voltage and the energy price for realizing the self-sensing function, need to be further investigated in future work, this proposed solution offers a new insight toward the designs of self-contained, flexible, and more informative PEH systems.

REFERENCES

[1] L. Gao, L. Teng, J. Liang, H. Wang, Y. Liu, and M. Fu, "A self-sensing synchronous electric charge extraction (SECE) solution for piezoelectric energy harvesting enhancement," in *2021 IEEE Applied Power Electronics Conference and Exposition (APEC)*, Jun. 2021, pp. 1393–1397.

[2] M. Lee, J. Yang, M.-J. Park, S.-Y. Jung, and J. Kim, "Design and analysis of Energy-Efficient Single-Pulse piezoelectric energy harvester and power management IC for Battery-Free wireless remote switch applications," *IEEE Trans. Circuits Syst. I Regul. Pap.*, vol. 65, no. 1, pp. 366–379, Jan. 2018.

[3] D. Wang, G. Yuan, G. Hao, and Y. Wang, "All-inorganic flexible piezoelectric energy harvester enabled by two-dimensional mica," *Nano Energy*, vol. 43, pp. 351–358, Jan. 2018.

[4] R. Subbaramaiah, S. A. Al-Jufout, A. Ahmed, and M. M. Mozumdar, "Design of Vibration-Sourced piezoelectric harvester for Battery-Powered smart road sensor systems," *IEEE Sens. J.*, vol. 20, no. 23, pp. 13 940–13 949, Dec. 2020.

[5] M. R. Elhebeary, M. A. A. Ibrahim, M. M. Aboudina, and A. N. Mohieldin, "Dual-Source Self-Start High-Efficiency microscale smart energy harvesting system for IoT," *IEEE Trans. Ind. Electron.*, vol. 65, no. 1, pp. 342–351, Jan. 2018.

[6] A. Abasian, A. Tabesh, N. Rezaei-Hosseinabadi, A. Z. Nezhad, M. Bongiorno, and S. A. Khajehoddin, "Vacuum-Packaged piezoelectric energy harvester for powering smart grid monitoring devices," *IEEE Trans. Ind. Electron.*, vol. 66, no. 6, pp. 4447–4456, Jun. 2019.

[7] Z. J. Chew, T. Ruan, M. Zhu, M. Bafleur, and J. Dilhac, "Single piezoelectric transducer as strain sensor and energy harvester using Time-Multiplexing operation," *IEEE Trans. Ind. Electron.*, vol. 64, no. 12, pp. 9646–9656, Dec. 2017.

[8] S. Du, Y. Jia, C. Zhao, G. A. J. Amaratunga, and A. A. Seshia, "A passive design scheme to increase the rectified power of piezoelectric energy harvesters," *IEEE Trans. Ind. Electron.*, vol. 65, no. 9, pp. 7095–7105, Sep. 2018.

[9] Z. J. Chew and M. Zhu, "Adaptive Self-Configurable rectifier for extended operating range of piezoelectric energy harvesting," *IEEE Trans. Ind. Electron.*, vol. 67, no. 4, pp. 3267–3276, Apr. 2020.

[10] K. Zhao, Y. Zhao, and J. Liang, "Live demo of a vibration-powered bluetooth sensor with running PFC power conditioning," in *2017 IEEE International Symposium on Circuits and Systems (ISCAS)*, May 2017, pp. 1–1.

[11] Y. C. Shu, I. C. Lien, and W. J. Wu, "An improved analysis of the SSHI interface in piezoelectric energy harvesting," *Smart Mater. Struct.*, vol. 16, no. 6, p. 2253, Oct. 2007.

[12] I. C. Lien, Y. C. Shu, W. J. Wu, S. M. Shiu, and H. C. Lin, "Revisit of series-SSHI with comparisons to other interfacing circuits in piezoelectric energy harvesting," *Smart Mater. Struct.*, vol. 19, no. 12, p. 125009, Oct. 2010.

[13] E. Lefeuvre, A. Badel, C. Richard, and D. Guyomar, "Piezoelectric energy harvesting device optimization by synchronous electric charge extraction," *J. Intell. Mater. Syst. Struct.*, vol. 16, no. 10, pp. 865–876, Oct. 2005.

[14] J. Liang, Y. Zhao, and K. Zhao, "Synchronized triple Bias-Flip interface circuit for piezoelectric energy harvesting enhancement," *IEEE Trans. Power Electron.*, vol. 34, no. 1, pp. 275–286, Jan. 2019.

[15] S. Chamanian, H. Uluşan, A. Koyuncuoğlu, A. Muhtaroğlu, and H. Külah, "An adaptable interface circuit with multistage energy extraction for Low-Power piezoelectric energy harvesting MEMS," *IEEE Trans. Power Electron.*, vol. 34, no. 3, pp. 2739–2747, Mar. 2019.

[16] K.-R. Cheng, H.-S. Chen, M. Lallart, and W.-J. Wu, "A 0.25μm HV-CMOS synchronous inversion and charge extraction (SICE) interface circuit for piezoelectric energy harvesting," in *2018 IEEE International Symposium on Circuits and Systems (ISCAS)*, May 2018, pp. 1–4.
[17] S. Fang, H. Xia, Y. Xia, Y. Ye, G. Shi, X. Wang, and Z. Chen, "An efficient piezoelectric energy harvesting circuit with Series-SSHI rectifier and FNOV-MPPT control technique," *IEEE Trans. Ind. Electron.*, vol. 68, no. 8, pp. 7146–7155, Aug. 2021.
[18] M. Meng, D. Wang, B. D. Truong, S. Trolier-McKinstry, S. Roundy, and M. Kiani, "A Multi-Beam Shared-Inductor reconfigurable Voltage/SECE mode piezoelectric energy harvesting interface circuit," *IEEE Trans. Biomed. Circuits Syst.*, vol. 13, no. 6, pp. 1277–1287, Dec. 2019.
[19] L. Teng, J. Liang, and Z. Chen, "Multiple charge extractions with Bias-Flip interface circuit for piezoelectric energy harvesting," in *2020 IEEE International Symposium on Circuits and Systems (ISCAS)*, Oct. 2020, pp. 1–5.
[20] D. A. Sanchez, J. Leicht, F. Hagedorn, E. Jodka, E. Fazel, and Y. Manoli, "A Parallel-SSHI rectifier for piezoelectric energy harvesting of periodic and shock excitations," *IEEE J. Solid-State Circuits*, vol. 51, no. 12, pp. 2867–2879, Dec. 2016.
[21] L. Wu, X. Do, S. Lee, and D. S. Ha, "A Self-Powered and optimal SSHI circuit integrated with an active rectifier for piezoelectric energy harvesting," *IEEE Trans. Circuits Syst. I Regul. Pap.*, vol. 64, no. 3, pp. 537–549, Mar. 2017.
[22] G. Shi, Y. Xia, X. Wang, L. Qian, Y. Ye, and Q. Li, "An efficient Self-Powered piezoelectric energy harvesting CMOS interface circuit based on synchronous charge extraction technique," *IEEE Trans. Circuits Syst. I Regul. Pap.*, vol. 65, no. 2, pp. 804–817, Feb. 2018.
[23] M. B. Khan, D. H. Kim, J. H. Han, H. Saif, H. Lee, Y. Lee, M. Kim, E. Jang, D. J. Joe, K. J. Lee, and Y. Lee, "A harvesting circuit for flexible Thin-Film piezoelectric generator achieving 562% energy extraction improvement with load screening," *IEEE Trans. Ind. Electron.*, vol. 68, no. 12, pp. 12 310–12 321, Dec. 2021.
[24] Z. Chen, M.-K. Law, P.-I. Mak, W.-H. Ki, and R. P. Martins, "Fully integrated Inductor-Less Flipping-Capacitor rectifier for piezoelectric energy harvesting," *IEEE J. Solid-State Circuits*, vol. 52, no. 12, pp. 3168–3180, Dec. 2017.
[25] S. Du and A. A. Seshia, "An inductorless Bias-Flip rectifier for piezoelectric energy harvesting," *IEEE J. Solid-State Circuits*, vol. 52, no. 10, pp. 2746–2757, Oct. 2017.
[26] S. Du, Y. Jia, C. Zhao, G. A. J. Amaratunga, and A. A. Seshia, "A fully integrated Split-Electrode SSHC rectifier for piezoelectric energy harvesting," *IEEE J. Solid-State Circuits*, vol. 54, no. 6, pp. 1733–1743, Jun. 2019.
[27] W. Q. Liu, A. Badel, F. Formosa, Y. P. Wu, and A. Agbossou, "Wideband energy harvesting using a combination of an optimized synchronous electric charge extraction circuit and a bistable harvester," *Smart Mater. Struct.*, vol. 22, no. 12, p. 125038, Nov. 2013.
[28] Z. J. Chew, T. Ruan, and M. Zhu, "Strain energy harvesting powered wireless sensor system using adaptive and Energy-Aware interface for enhanced performance," *IEEE Trans. Ind. Inf.*, vol. 13, no. 6, pp. 3006–3016, Dec. 2017.
[29] H. Xia, Y. Xia, Y. Ye, L. Qian, and G. Shi, "Simultaneous wireless strain sensing and energy harvesting from multiple Piezo-Patches for structural health monitoring applications," *IEEE Trans. Ind. Electron.*, vol. 66, no. 10, pp. 8235–8243, Oct. 2019.
[30] J. Liang and W.-H. Liao, "Improved design and analysis of Self-Powered synchronized switch interface circuit for piezoelectric energy harvesting systems," *IEEE Trans. Ind. Electron.*, vol. 59, no. 4, pp. 1950–1960, Apr. 2012.

Linglong Gao has received his B.E.degree in Communication Engineering from Shanghai Maritime University in June 2019. He is now working toward his Ph.D degree at ShanghaiTech University, China. His research interests include piezoelectric energy harvesting and the Internet of Things.

Li Teng has received his B.S. degree in Microelectronics from Hefei University of Technology in 2015. After graduation, he worked as an analog IC design engineer in Wuxi ETEK Microelectronics Co., Ltd. He is now working toward the Ph.D. degree at Shanghaitech University. His research interests cover analog/mixed-signal IC design.

Minfan Fu (Senior Member, IEEE) received the B.S., M.S., and Ph.D. degrees in electrical and computer engineering from the University of MichiganShanghai Jiao Tong University Joint Institute, Shanghai Jiao Tong University, Shanghai, China, in 2010, 2013, and 2016, respectively. From 2016 to 2018, he was a Postdoctoral with the Center for Power Electronics Systems, Virginia Polytechnic Institute, and State University, Blacksburg, VA, USA. He is currently an Assistant Professor at the School of Information Science and Technology, ShanghaiTech University, Shanghai, China. He holds one U.S. patent, and three Chinese patents, and has authored or co-authored more than 50 papers in prestigious IEEE journals and conferences. His research interests include megahertz wireless power transfer, high-frequency power conversion, high-frequency magnetic design, and the application of wide-bandgap devices. Dr. Fu is currently an Associate Editor for the IEEE IES Industrial Electronics Technology News and serves as the Section Chair of several conferences, such as IECON, IPEMC, and VEH. His conference paper for IECON 2019 won the IES-SYPA Competition. He is the Tutorial Speaker for IPEMC 2020 and ISIE 2020.

Haoyu Wang (Senior Member, IEEE) received a bachelor's degree (with Distinguished Hons.) in electrical engineering from Zhejiang University, Hangzhou, China, in 2009, and a Ph.D. degree in electrical engineering from the University of Maryland at College Park, College Park, MD, USA, in 2014. In 2014, he joined the School of Information Science and Technology, ShanghaiTech University, Shanghai, China, where he is currently a tenured Associate Professor. His research interests include power electronics, plug-in electric and hybrid electric vehicles, the applications of wide-bandgap semiconductors, renewable energy harvesting, and power management integrated circuits. Dr. Wang is an Associate Editor for IEEE Transactions on Industrial Electronics, IEEE Transactions on Transportation Electrification, and CPSS Transactions on Power Electronics and Applications.

Junrui Liang (Senior Member, IEEE) received the B.E. and M.E. degrees in instrumentation engineering from Shanghai Jiao Tong University, Shanghai, China, in 2004 and 2007, respectively, and the Ph.D. degree in mechanical and automation engineering from The Chinese University Hong Kong, Hong Kong, China, in 2010. He is currently an Associate Professor with the School of Information Science and Technology, ShanghaiTech University, Shanghai, China. His research interests include energy conversion and power conditioning circuits, kinetic energy harvesting and vibration suppression, IoT devices, and mechatronics. Dr. Liang is an Associate Editor of IET Circuits, Devices and Systems and the General Chair of the 2nd International Conference on Vibration and Energy Harvesting Applications (VEH) 2019.